Ecological Informatics 33 (2016) 32–44

Contents lists available at ScienceDirect

Ecological Informatics

journal homepage: www.elsevier.com/locate/ecolinf

Quantitative assess the driving forces on the grassland degradation in the Qinghai–Tibet Plateau, in China

Zhaoqi Wang [a], Yanzhen Zhang [a], Yue Yang [a], Wei Zhou [b], Chencheng Gang [c], Ying Zhang [a], Jianlong Li [a,*], Ru An [d], Ke Wang [e], Inakwu Odeh [f], Jiaguo Qi [g]

[a] Department of Ecology, School of Life Science, Nanjing University, Nanjing, PR China
[b] School of River & Ocean Engineering, Chongqing Jiaotong University, Chongqing, PR China
[c] Institute of Soil and Water Conservation, CAS, Yangling, PR China
[d] School of Earth Science and Engineering, Hehai University, Nanjing, PR China
[e] Hutai Middle school, Xining, PR China
[f] Department of Environmental Sciences, Faculty of Agricultural and Environment, The University of Sydney, Sydney, Australia
[g] The Center for Global Change & Earth Observations, Michigan State University, East Lansing, USA

ARTICLE INFO

Article history:
Received 13 November 2015
Received in revised form 8 January 2016
Accepted 31 March 2016
Available online 8 April 2016

Keywords:
Grassland degradation
Climate variation
Human activities
Net primary production
Qinghai–Tibet Plateau

ABSTRACT

Grassland degradation in the Qinghai–Tibet Plateau (QTP), has attracted considerable concern because of its negative influence on the development of the local economy and the ecological security of China. Climate and human activities are considered as the main driving forces of grassland degradation. However, distinguishing their respective contributions to grassland degradation is a challenge. This study used the Carnegie–Ames–Stanford Approach model, which coupling remote sensing (e.g. NDVI, LAI, near and mid-infrared bands) and meteorological data (precipitation, temperature and radiation), was adopted to simulate the actual and potential NPP in the QTP from 2001 to 2013. The difference between potential NPP and actual NPP was used to represent the influence of human activities. Results showed that nearly 38.8% of the total grassland area underwent degradation, whereas 61.2% experienced restoration. Furthermore, 56.7% of the degraded grassland areas were influenced by climate, and 19.9% were affected by human activities. The restored areas induced by human activities, climate variation, and the combination of the two factors accounted for 28.6%, 12.8% and 19.9% with an increases in NPP of 5923.4, 3188.1 and 5959.2 GgC, respectively. Therefore, climate was the principal driving force of grassland degradation, whereas human activities were the dominant factor in grassland restoration. Climate and human activities, as the potential driving force in grassland NPP variations, should be fully understood by a long term monitoring and the main causes exploring in its dynamics. In addition, the uncertainty of the driving forces should be clarifying immediately in the future, and provide scientific basis for policies and plans making in grassland management.

1. Introduction

As one of the most common vegetation types, i.e., accounting for 20% of the land surface area of the world, grassland has a key role in ecology, food security (Conant et al., 2001), carbon balancing, and global climate change (Piao et al., 2009). The grassland in China covers approximately 4 million km^2, which is nearly 40% of the country's land area. Global warming and increasing human activities have significantly affected the natural ecosystems in many regions of the world (Gao et al., 2013). In China, approximately 90% of the total grassland area has been degraded to a certain extent (Nan, 2005) because of global warming (Yu et al., 2012), population growth (Nan, 2005), and excessive land use (Harris, 2010). To date, numerous studies have been conducted to analyze grassland degradation worldwide (Harris, 2010).

The Qinghai–Tibet Plateau (QTP), which is one of the largest and most unique geographical units on Earth, has a mean elevation of more than 4000 m above sea level (a.s.l.). This plateau is known as the "third pole" of the Earth and has a significant role in maintaining the ecological security of China (Qiu, 2008) and the global carbon cycle (Piao et al., 2012; Zhao et al., 2006), accounting for approximately 2.5% of the global soil carbon pool (Genxu et al., 2002). The region is approximately 2.5 million km^2, which is nearly 25% of the area of China. Grassland is the dominant vegetation type in the QTP and nearly half (44%) of grasslands in China, which is also accounts for 6% of the total grassland areas of the world (Scurlock and Hall, 1998; Tan et al., 2010). The grassland ecosystem in the QTP is extremely sensitive to climate variation and human activities because of its vulnerability and the alpine condition in the region (Kato et al., 2004; Piao et al., 2006).

Climate and human activities are considered the main driving forces of grassland degradation (Chen et al., 2014; Chen et al., 2013; Wessels et al., 2008). Distinguishing between the contributions of these two

* Corresponding author.
E-mail address: lijianlongnju@163.com (J. Li).

http://dx.doi.org/10.1016/j.ecoinf.2016.03.006
1574-9541/

factors is difficult but is urgently required in quantitative methods for assessing the respective effects of climate and human activities on grassland degradation (Wang et al., 2010; Wessels et al., 2008). Currently, the newly Landsat-8 satellite was employed to detect the grassland degradation in the QTP (Fassnacht et al., 2015), other indirect methods that are used to assess the influence of human activities on ecosystems include the normalized difference vegetation index (NDVI), Wessels (Wessels et al., 2004) proposed a Land capability units coupling NDVI method, making it possible to distinguish natural physical variations from human influences; and Li applied a using the NDVI-based residual trend method to investigate the human and climate forces in vegetation changes in inner Mongolia (Li et al., 2012). Rojstaczer (Rojstaczer et al., 2001) incorporates contemporary data to estimate human use of terrestrial net primary production to measure of human impact on the biosphere and hydrosphere. While, Harberl (Haberl et al., 2007) presents a comprehensive assessment of global human appropriation of net primary productivity to estimate human impact on ecosystems. Several studies have assessed the contributions of these two factors by selecting net primary production (NPP) as an indicator because of its significance in indicating grassland degradation and the status of ecological processes. Xu's work focused on the desertification, and the assessing methods were built based on the slope of NPP and scenarios simulation (Xu et al., 2009), Zhou and Gang expanded study region to global and regional scale, and this method was applied to detect grassland degradation (Gang et al., 2014; Zhou et al., 2015). Consequently, NPP coupled scenario simulation methodology has been successfully applied in detecting land degradation.

Degradation is not only a retrogressive succession process of the grassland ecosystem under the influences of human activities and natural factors (Li, 1997), but also a relative state on the time series. Identifying the respective contributions of climate and human activities is important because the main driving force, location, and extent of grassland degradation should be primarily clarified. The former studies have only identified human activities in the regions affected by land degradation, and the respective roles of climate and human activities in land degradation remain unclear (Haberl et al., 2007; Li et al., 2012; Wessels et al., 2004), and the recent studies devoted to differentiate the relative contribution in grassland productivities dynamics. However, it still remains uncertain to calculate potential NPP by using the statistic model (Gang et al., 2014; Zhou et al., 2015). In this study, NPP was selected as the indicator to analyze the relative role of driving factors in grassland productivity dynamics in which minimal attention has been given to the grassland ecosystem of the QTP despite the importance of this region. Consequently, a scenario simulation method was established on the basis of the slope of NPP. We integrated Carnegie–Ames–Stanford Approach (CASA) model to simulate actual NPP and potential NPP to reflect grassland degradation and restoration, and reduce the uncertainties remained in the methodology. Most importantly, the principal driving forces of grassland degradation or restoration, their corresponding NPP variations, and the extent of the affected area were identified over time in the QTP. All these works were designed to provide theoretical and methodological bases for policy making and optimizing ecosystem management in grasslands.

2. Materials and methods

2.1. Study area

The QTP is located in southwest China (26.5–39.5°N, 78.3–103.1°E). This plateau has an average altitude of 4000 m a.s.l. Alpine and subalpine meadows are the dominant vegetation types in the QTP (covers over 40% of the plateau area) (Bartholomé and Belward, 2005). Other grassland types include alpine and sub-alpine meadow, meadow, alpine and sub-alpine plain grasslands, as well as slope grassland, plain grassland and desert grassland (Fig. 1). The mean temperature in the QTP is generally lower than −10 °C during the coldest month and lower than 10 °C during the warmest month (Piao et al., 2011). The QTP has experienced significant warming since the mid-1950s, with the mean annual temperature increasing by 0.3 °C per decade (Piao et al., 2012). The southeast QTP is the wettest area with an annual precipitation over 1000 mm. Meanwhile, annual precipitation in the driest northwest area is less than 50 mm (Zheng, 1996). The QTP is essentially the source of all of the major rivers in Asia, including the Yangtze River, the Yellow River, and the Lancang River, which are considered as “China water tower”.

2.2. Remote sensing data

The Moderate-resolution imaging spectroradiometer (MODIS) MOD13A2 and MOD15A2 dataset products from 2001 to 2013, with a spatial resolution of 1 km and a temporal scale of 16 days, were obtained from the Level 1 and Atmosphere Archive and Distribution System Web of NASA (http://ladsweb.nascom.nasa.gov/data/search.html). The MOD13A2 dataset used in the study including NDVI, near and mid-infrared bands while the MOD15A2 dataset including LAI. The NDVI dataset was successful applied in estimation of actual evapotranspiration and achieved valuable outcome recently (Rahimi et al., 2015). The maximum value composite method (Holben, 1986) was employed to merge the days in the NDVI and LAI data and to generate monthly data. Moreover, the LAI dataset was performed minimum value composite to retrieve the input parameter. Radiation correction and geometric correction were already performed on the original NDVI dataset. The coordinate and projection system used were the World Geodetic System 1984 and the Albers equal area conic projection respectively.

2.3. Meteorological data

The meteorological data used included the average monthly temperature data and monthly precipitation data from 97 meteorological stations, as well as the total solar radiation data from 11 stations in study area from 2001 to 2013. These data were collected from the China Meteorological Data Sharing Service System (http://cdc.cma.gov.cn/). The meteorological data were then interpolated by using the ordinary Kriging interpolation method to generate monthly raster data with a spatial resolution of 1 km. The coordinate system and projection were the same as those for remote sensing data. The radiation and temperature based method has been successfully applied in estimating evapotranspiration and achieved fruitful outcomes (Valipour, 2015a; Valipour, 2015c; Valipour and Eslamian, 2014). Moreover, the radiation-based method was proved that could obtain highest precision of estimation in the parameters if used for suitable and specific weather conditions (Valipour, 2015b; Valipour, 2015d). Notably, radiation-based method provides a guideline of potential application of radiation and temperature data. The current study also used the potential advantage of radiation and temperature datasets for specific weather condition, expecting to obtain promising results.

2.4. Grassland classification data

The Global Land Cover 2000 (GLC2000) was produced by an international partnership that consisted of 30 research groups under the coordination of the Joint Research Center of the European Commission in 2000 (Bartholomé and Belward, 2005). The GLC2000 database was based on the data from the VEGETATION sensor placed on-board SPOT 4 and comprise 22 land cover classes with a resolution of 1 km. The study area was extracted from the GLC2000 database and classes 8–12 and 22 were selected as grasslands. The GLC2000 database is available at http://bioval.jrc.ec.europa.eu/products/glc2000/data_access.php.

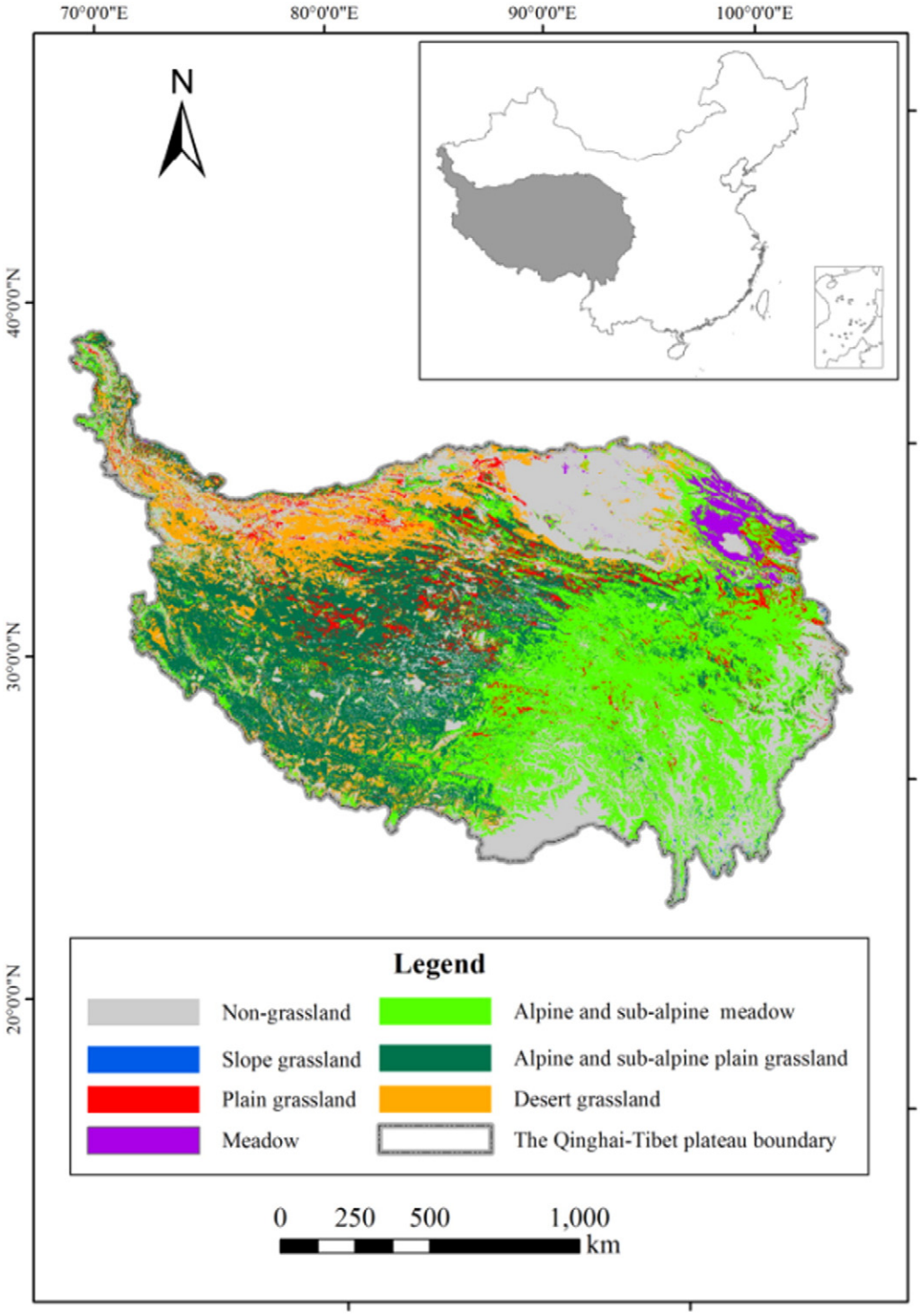

Fig. 1. The location of study area and the distribution of grassland type in QTP.

2.5. Statistical data

The livestock and population data of counties in the QTP from 2001 to 2013 was collected from Qinghai statistical yearbook, Tibet statistical yearbook and Gansu development yearbook.

2.6. Calculating actual NPP and potential NPP

Actual NPP was calculated by using the CASA model, which is a light use efficiency model (Potter et al., 1999; Potter et al., 1993) with remote sensing and meteorological data as the driving parameters. The basic principle of the CASA model includes two variables, namely: absorbed photosynthetically active radiation (APAR) and light energy conversion (ε). NPP is the product of APAR and ε.

$$NPP(x,t) = APAR(x,t) \times \varepsilon(x,t) \quad (1)$$

where x is the spatial location, t is time, APAR (x, t) represents the canopy-absorbed incident solar radiation of pixel x in t time (MJ m^{-2}), and ε (x, t) represents the actual light use efficiency (g C/MJ) of pixel x in t time. APAR (x, t) and ε (x, t) can be calculated

by using Eqs. (2) and (5), respectively.

$$APAR(x,t) = SOL(x,t) \times FPAR(x,t) \times 0.5 \quad (2)$$

where SOL (x, t) is the total solar radiation (MJ m^{-2}) of pixel x in t time, and FPAR (x, t) is the fraction of the incoming photosynthetically active radiation (FPAR) intercepted by green vegetation and determined by NDVI. The factor of 0.5 accounts for the fraction of the total solar radiation available for vegetation in the PAR waveband (0.4–0.7 μm).

$$FPAR(x,t) = \min\left\{\left(\frac{SR(x,t)}{SR_{max}-SR_{min}} - \frac{SR_{min}}{SR_{max}-SR_{min}}\right), 0.95\right\} \quad (3)$$

where SR(x,t) represent the simple ratio of pixel x in t time, SR_{max} and SR_{min} represent the maximum and minimum value of SR.

$$SR(x,t) = [1 + NDVI(x,t)]/[1-NDVI(x,t)] \quad (4)$$

where NDVI(x,t) is the NDVI value of pixel x in t time.

$$\varepsilon(x,t) = T_{\varepsilon 1}(x,t) \times T_{\varepsilon 2}(x,t) \times W_{\varepsilon}(x,t) \times \varepsilon_{max} \quad (5)$$

where $T_{\varepsilon 1}(x,t)$ and $T_{\varepsilon 2}(x,t)$ represent the effects of low and high temperature stress, respectively; they can be calculated by using Eq. (6) and (7). $W_{\varepsilon}(x,t)$ represents the effects of water stress (Potter et al., 1993), and ε_{max} is the maximum possible efficiency. According to a previous study (Zhu et al., 2006), the value of ε_{max} is set to 0.542 for grassland in the current study.

$$T_{\varepsilon 1}(x,t) = 0.8 + 0.02 \times T_{opt}(x) - 0.0005 \times [T_{opt}(x)]^2 \quad (6)$$

$$T_{\varepsilon 2}(x,t) = 1.184/\{1 + \exp[0.2 \times (T_{opt}(x) - 10 - T(x,t))]\} \times 1/\{1 + \exp[0.3 \times (-T_{opt}(x) - 10 - T(x,t))]\} \quad (7)$$

where T (x, t) is the air temperature of pixel x at month t, and T_{opt} (x) is the optimum air temperature when the vegetation biomass reaches the maximum value.

$$W_{\varepsilon}(x,t) = 0.5 + 0.5 \times PPT(x,t)/PET(x,t) \quad (8)$$

where PPT (x, t) and PET (x, t) are the precipitation and potential evapotranspiration of location x at month t, respectively; PET (x, t) can be calculated according to the CASA soil moisture sub-model (Potter et al., 1993); and W_{ε} is range from 0.5 for arid and 1 for wet.

Potential NPP was calculated with the same method as actual NPP but they differ in FPAR. In this study, the potential FPAR (PFPAR) was calculated by the potential leaf area index (PLAI) and meteorological data. The model can be expressed as follows:

$$PFPAR = 1 - e^{-k*PLAI} \quad (9)$$

where k = 0.5, and the PLAI can be calculated by the following:

$$PLAI = LAI_{min} + fsw \times fst \times (LAI_{max} - LAI_{min}) \quad (10)$$

where the maximum and minimum values in a month was defined as LAI_{max} and LAI_{min}, respectively. fsw was used to estimate the dynamics of water by remote sensing data (Xiao et al., 2005), which was calculated according Eq. (11); and fst is the temperature stress:

$$fst = \frac{(T-T_{min})(T-T_{max})}{(T-T_{min})(T-T_{max}) - (T-T_{opt})} \quad (11)$$

$$fsw = \frac{1-LSWI}{1+LSWI} \quad (12)$$

where T_{max} and T_{min} are the maximum and minimum air temperatures in a month, respectively; and T_{opt} is the optimum air temperature, as previously described. $LSWI_{max}$ is the maximum value at the month scale for each pixel. LSWI is computed as follows:

$$LSWI = \frac{\rho_{NIR} - \rho_{MIR}}{\rho_{NIR} + \rho_{MIR}} \quad (13)$$

where ρ_{NIR} and ρ_{MIR} represent the albedo of near and mid-infrared bands of the MODIS image in this study, respectively.

2.7. Grassland dynamic assessment

NPP is a fundamental indicator of vegetation productivity that can reflect vegetation dynamics and the status of ecological processes. Thus, NPP was selected to assess grassland degradation or restoration by using the ordinary least-square method. The formula is described as follows:

$$Slope = \frac{n \times \sum_{i=1}^{n}(i \times Var_i) - \left(\sum_{i=1}^{n} i\right)\left(\sum_{n=1}^{n} Var_i\right)}{n \times \left(\sum_{i=1}^{n} i^2\right) - \left(\sum_{i=1}^{n} i\right)^2} \quad (14)$$

where n is the number of years, and i is the sequence number of the year. Var_i is the total annual NPP in year i. A negative slope value indicates a degradation trend, whereas a positive slope value indicates a restoration trend.

The total increased or decreased NPP at each pixel during the study period can be identified by using the following formula:

$$\Delta NPP = (n-1) \times slope \quad (15)$$

where n is the number of years, e.g., if the year is from 2001 to 2013, then n = 13.

The significance of the variation tendency was determined by an F-test to represent the confidence level of variation. The calculation for statistics is expressed as follows:

$$F = U \times \frac{n-2}{Q} \quad (16)$$

$$U = \sum_{i=1}^{n}(\hat{y}_i - \overline{y})^2 \quad (17)$$

$$Q = \sum_{i=1}^{n}(y_i - \hat{y}_i)^2 \quad (18)$$

$$\hat{y}_i = Slope \times i + b \quad (19)$$

$$b = \overline{y} - Slope \times \overline{i} \quad (20)$$

where U is the residual sum of the squares; Q is the regression sum; $\hat{y}_i$ is the regression value, which can be calculated by Eqs. (17)–(19); y_i is the average data of year i, $\overline{y}$ is the mean data over n years; and b is the intercept of the regression formula.

The variation tendency was classified into the following six levels on the basis of the F-test results: Extremely Significant Decrease (ESD, slope < 0, p < 0.01); Significant Decrease (SD, slope < 0, 0.01 < p < 0.05); Not Significant Decrease (NSD, slope < 0, p > 0.05); Not Significant Change (NSC, slope = 0); Not Significant Increase (NSI, slope > 0, p > 0.05); Significant Increase (SI, Slope > 0, 0.01 < p < 0.05); and Extremely Significant Increase (ESI, slope > 0, p < 0.01).

Table 1
The scenarios of the relative role of climate and human activities on grassland restoration and degradation.

	Scenario	S_C	S_H	Relative role of climate (%)	Relative role of human activities (%)
Grassland restoration ($S_A > 0$)	Scenario 1	>0	>0	100	0
	Scenario 2	<0	<0	0	100
	Scenario 3	>0	<0	Combined the two factors	Combined the two factors
	Scenario 4	<0	>0	Error	Error
Grassland degradation ($S_A < 0$)	Scenario 5	>0	>0	0	100
	Scenario 6	<0	<0	100	0
	Scenario 7	<0	>0	Combined the two factors	Combined the two factors
	Scenario 8	>0	<0	Error	Error

2.8. Correlation analysis

The Pearson correlation coefficient was employed to reflect the long-term dynamic of two variables at a given time n (Eq.(21)).

$$r = \frac{n \times \sum_{i=1}^{n}(x_i \times y_i) - \left(\sum_{i=1}^{n} x_i\right)\left(\sum_{n=1}^{n} y_i\right)}{\sqrt{n \times \left(\sum_{i=1}^{n} x_i^2\right) - \left(\sum_{i=1}^{n} x_i\right)^2}\sqrt{n \times \left(\sum_{i=1}^{n} y_i{}^2\right) - \left(\sum_{i=1}^{n} y_i\right)^2}} \quad (21)$$

where n is the sequential year, in this study, x_i and y_i represents NPP and year i, respectively.

2.9. Establishing scenarios

Three kinds of NPP were introduced, and the dynamics of NPP were based on Eq. (15). The scenarios were on the basis of the hypothesis that grassland productivity dynamics are only affected by climate and human activities. First, actual NPP (NPP_A), which was calculated by using the CASA model, indicated the actual situation in which grassland productivity was affected by both climate and human activities. A positive slope value (S_A) suggested that restoration occurs, whereas a negative slope value suggested that degradation occurred.

Second, potential NPP (NPP_C) indicated the hypothetical situation in which grassland productivity was affected by climate. A positive slope value (S_C) suggested that the climate increased grassland productivity, whereas a negative NPP value suggested that climate decreased grassland productivity.

Third, human-induced NPP (NPP_H), which was calculated as the difference between NPP_C and NPP_A ($NPP_H = NPP_C - NPP_A$), hypothesized that lost NPP was affected by human activities. A positive slope value (S_H) suggested that human activities decreased grassland productivity. By contrast, a negative slope value (S_H) suggested that human activities increased grassland productivity.

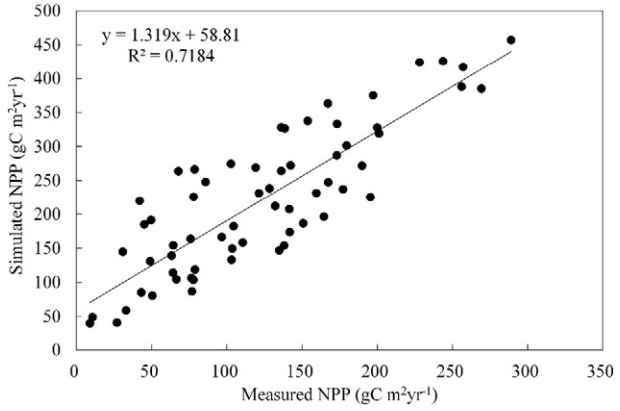

Fig. 2. The validation of simulated NPP by CASA-model.

Therefore, eight scenarios were established on the basis of the concepts of S_A, S_C, and S_H. The situation of $S_A > 0$ indicated that grassland restoration occurred, and $S_A < 0$ indicated that grassland degradation occurred during the study period.

Under the $S_A > 0$ situation, scenarios 1 and 5 ($S_C > 0$, $S_H > 0$) denoted that NPP_C increased ($S_C > 0$), but the loss of NPP is increasing ($S_H > 0$) means the human activity harm to grassland. We could then consider that the increased NPP was solely attributed to climate. Similarly, under the $S_A < 0$ situation, scenario 1 denoted the degradation was solely caused by human activities.

Under the $S_A > 0$ situation, scenarios 2 and 6 ($S_C < 0$, $S_H < 0$) denoted that restoration was solely attributed to human activities. On the contrary, under the $S_A < 0$ situation, scenario 2 denoted the degradation was solely attributed to climate.

Under either the $S_A > 0$ or $S_A < 0$ situation, scenarios 3 and 7 ($S_C > 0$, $S_H < 0$) denoted that restoration or degradation was affected by both climate and human activities.

In scenarios 4 and 8 ($S_C < 0$, $S_H > 0$), both climate and human activities were not the dominant factor in grassland restoration or degradation. This situation was not analyzed in this study to avoid uncertainties. The scenario simulations are shown in Table 1.

2.10. Field survey of NPP

A total of 63 field survey data, which were derived from the sampling plot, were used to validate the NPP simulated by the CASA model in August of 2013 and August of 2012. We selected nine quadrats (1 m × 1 m) evenly in each sampling plot (10 m × 10 m) and harvested the aboveground plants in each quadrat. Nine soil cores drilled by a soil auger (8 cm in diameter and 30 cm in depth) were then collected to determine the belowground biomass in a sampling plot. The belowground biomass samples were soaked in deionized water and filtered with a mesh sieve (0.5 mm) in laboratory. Plant biomass was dried to a constant weight at 65 °C. The average biomass value of the 9 quadrats was converted into carbon content by product with a factor of 0.45 (Fang et al., 1996).

3. Results

3.1. Validating the simulated NPP

Given that the field survey data were collected in August, the sum of NPP, which was simulated by the CASA model from January to August in 2012 and 2013, was compared with the measured NPP. The correlation between the observed NPP and the simulated NPP ($R^2 = 0.7024$, $p < 0.01$) showed that the CASA-model exhibited satisfactory accuracy

Table 2
Mann–Kendall test of climatic change trend.

	ANPP	HNPP	PNPP
Slope	0.27	−1.40	−1.24
R^2	0.02	0.19	0.08
Z value	0.43	−1.65**	−1.16

** The absolute value of Z passed the significance testing at the confidence level of 95%.

in estimating actual NPP (Fig. 2). The simulated NPP was larger than the measured one in some extent. However, these uncertainties brought by the difference could ignore in the trends analyst of NPP.

3.2. NPP_A, NPP_C and NPP_H changes in QTP grassland

The Mann–Kendall test was performed in the trend analysis of the QTP from 2001 to 2013 (Table 2). On the whole, the ANPP exhibits a slight increasing trend, while a decreasing trend was observed in the HNPP and PNPP. The HNPP was present significantly decreasing at the confidence level of 95%. The others did not reach the significant level. The detail of the NPP spatial variation and its significance are exhibited in Fig. 3. The total NPP_A exhibited an increasing trend, occupying 41.4% of the QTP grassland area, with an annual increment of 1.63 g C m^{-2}, such a trend mainly occurred in small parts of the northeastern, western, and southwestern QTP (Fig. 3A-1). The ESI and SI areas accounted for 4.9% and 7.0% of the QTP grassland area, respectively (Fig. 3A-2). By contrast, 27.3% of the total grassland area decreased

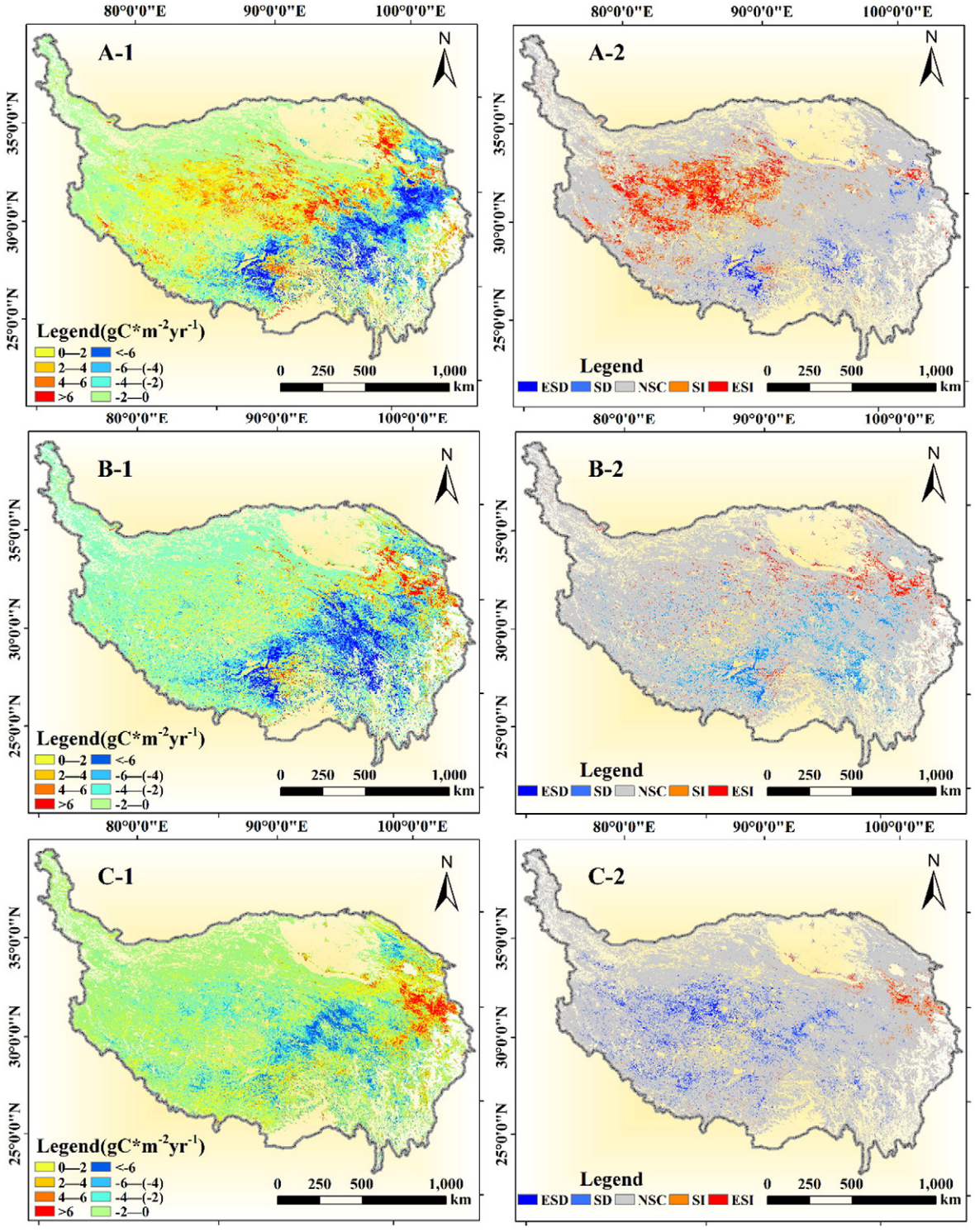

Fig. 3. The spatial variation trend of grassland NPP at different significance levels during 2001–2013. A-1, B-1 and C-1 are the slope of NPP_A, NPP_C and NPP_H, A-2, B-2 and C-2 corresponding its significance levels.

by 3.33 g C $m^{-2}y^{-1}$, as mainly observed in the eastern and southeastern QTP. Similarly, the ESD and SD areas accounted for 1.0% and 1.9% of the QTP grassland area, respectively. The remaining areas did not demonstrate a significantly increasing or decreasing trend.

According to the slope of NPP_C (Fig. 3B-1), the region that exhibit decreasing trends was larger than that with increasing trends (38.2% vs 18.7%). The increasing region typically occurred in the northeastern QTP, which enhanced at a rate of 2.54 g C $m^{-2}y^{-1}$. The ESI and SI regions occupied 1.2% and 2.2% of the QTP grassland area, respectively. The decreasing region all over the QTP, especially in the south and southeast, had a decreasing rate of 3.6 g C $m^{-2}y^{-1}$, the observed ESD and SD regions accounted for 2.2% and 4.0% of the QTP grassland, respectively (Fig. 3B-2).

NPP_H was high in relation to NPP_A and NPP_C according to the hypothesis. The results of the NPP_H slope demonstrated that 18.1% of the total grassland area experienced an increasing trend (Fig. 3C-1), which was mostly observed in the eastern QTP and had an increasing rate of 2.18 g C $m^{-2}y^{-1}$. The significant test showed that the ESI and SI regions only accounted for 0.5% and 1.1% of the QTP grassland area, respectively. Meanwhile, 42.1% of the QTP grassland area decreased at an annual rate of 3.07 g C m^{-2}, which was mainly founded in mid-east. The ESD and SD areas occupied 2.1% and 4.9% of the QTP grassland area, respectively (Fig. 3C-2).

3.3. Respective roles of climate and human activities in the QTP grassland

The spatial distribution of grassland NPP change affected by climate and human activities was analyzed. The observed degraded grassland area was 4.23×10^5 km^2, which accounted for 38.8% of the total grassland area. The climate-dominated grassland degradation region (CDD) was typically observed in parts of south, northeast corner, and east of the QTP, accounting for 56.7% of the total degraded grassland. By contrast, the central and southwestern parts of the QTP were mostly characterized by human-dominated grassland degradation (HDD) and accounted for 19.9% of the total degraded grassland. Both of the two factors dominated grassland degradation (BDD) accounted for 23.4% of the total degraded grassland, which was mainly found in the central and western parts of the QTP.

Table 3
The contribution of relative role of climate and human activities in terms of area, average NPP and total NPP (1 Gg = 10^9 g).

Dominated factor	Area(10^5 km2)	NPP variation rate (gC * m^{-2} $year^{-1}$)	Total NPP (GgC)
CDI	1.39	1.87	3118.06
HDI	3.12	1.58	5923.44
BDI	2.17	2.29	5959.20
CDD	2.40	−2.59	−7480.32
HDD	0.84	−2.29	−2314.32
BDD	0.99	−3.69	−4389.12

Fig. 4 shows the contributions of climate and human activities to grassland degradation in terms of NPP. The total grassland NPP decreased by up to 14,183.76 GgC from 2001 to 2013. Climate led to a loss of 7480.32 GgC, which accounted for 52.7% of the total loss carbon. By contrast, the NPP decrease induced by human activities was 2314.32 GgC, which accounts for 16.3% of the total loss carbon. The NPP decrease induced by the combination of the two factors was 4389.12 GgC, which occupied 30.9% of the total loss carbon. In summary, climate had a dominant role in driving grassland degradation.

The observed restored grassland area was 6.68×10^5 km^2, which accounted for 61.2% of the total grassland area. The area of climate-dominate grassland increase (CDI) is 1.4×10^5 km^2, which accounted for 20.8% of the total restoration area. This region was typically observed in the northeastern QTP. The area of human activities-dominate grassland increase (HDI) was 3.1×10^5 km^2, which occupied 46.7% of the

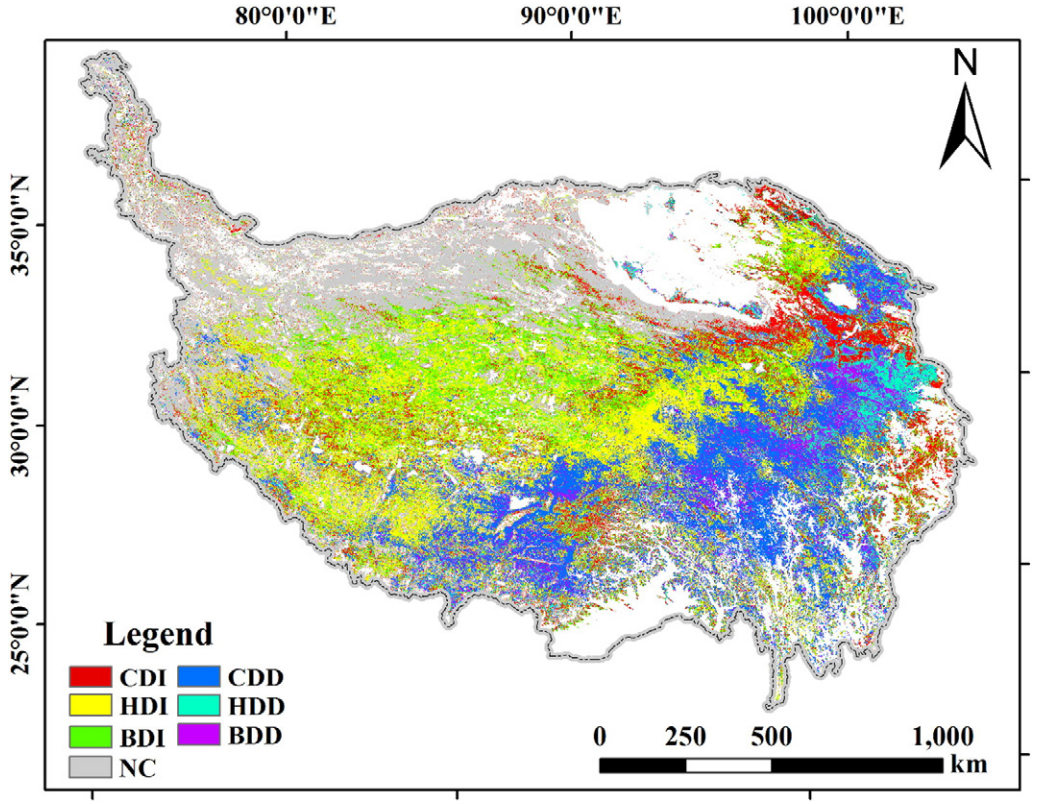

Fig. 4. The spatial distribution of climate, human activities and both of the two effects on the QTP grassland.

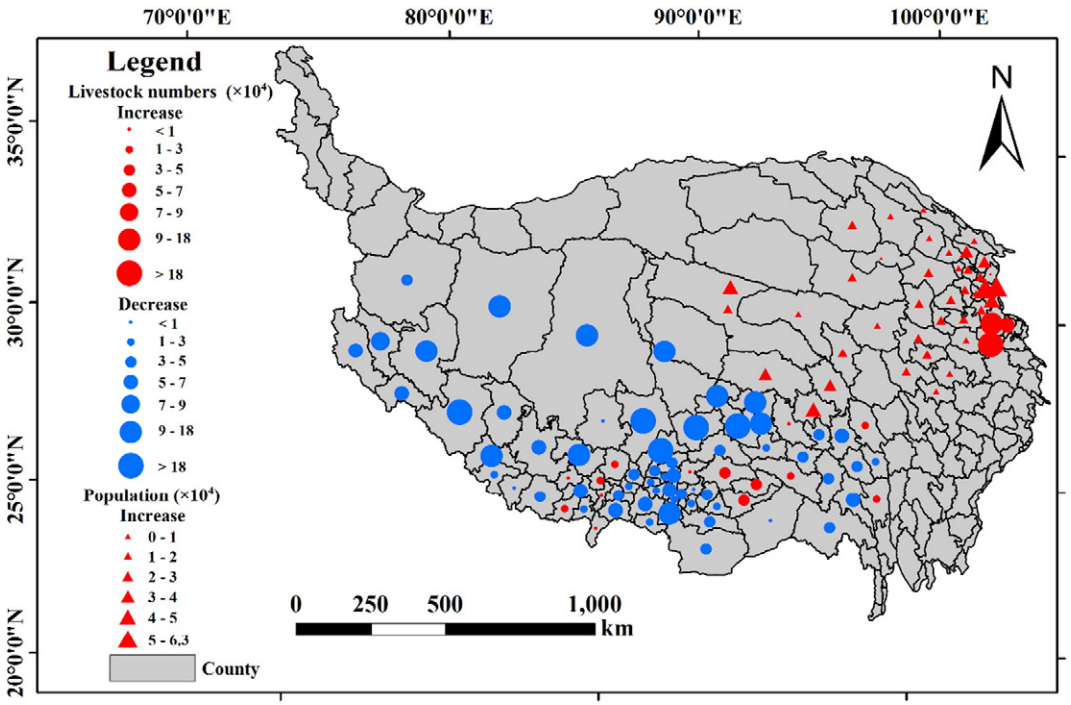

Fig. 5. The spatial–temporal distribution of livestock and population in the QTP from 2001 to 2013.

total restoration area and was generally located in the central and southwestern QTP. On the contrary, 32.5% of the total restoration area was attributed to both of the two factors dominated increase (BDI). This region was typically observed in the west, middle, and a small part of northeast of the QTP.

The total grassland NPP increased by 15,000.70 GgC because of the grassland restoration from 2001 to 2013. Climate induced grassland restoration accounted for 20.8% of the total grassland NPP restoration. Human activities and the combined factors indicated 5923.44 and 5959.20 GgC, accounting for 39.5% and 39.7% of the total grassland NPP restoration (Table 3), respectively. Both of the two factors led to the maximum NPP restoration; however, human activities could be considered the dominant factor in grassland restoration from 2001 to 2013.

We collected the livestock and population data of 101 counties in the QTP from 2001 to 2013, the rest counties were absence of data (Fig. 5). Generally, the livestock experienced decreasing trend in the southern and southwestern QTP, and the population were increased in the northeastern QTP. We think the results could interpret the outcome of Fig. 4 in some extent. The available data indicated that the livestock decreased at a total number of 4.09 million heads in the QTP from 2001 to 2013. Therefore, we speculate the human activities induced grassland increasing might attributed to the decrease of livestock. The human induced grassland degradation was observed in a part of the northeastern QTP, this situation coincident with the statistical data which indicated the population present increased trend, and livestock increased near 0.40 million heads in the same region. Therefore, the human induced grassland degradation most likely due to population growth and overgrazing. We addressed the effect of climate factors on NPP in Section 3.4 and 3.5.

3.4. Influence climate factors on NPP_A

In this study, the interpolated meteorological data indicate that 90.5%, 53.9%, and 32.9% of the grassland area in the QTP experienced an increasing trend in temperature, precipitation, and radiation, respectively (Fig. 6). Temperature increased by approximately 0.6 °C from 2001 to 2013. Meanwhile the increase in precipitation and

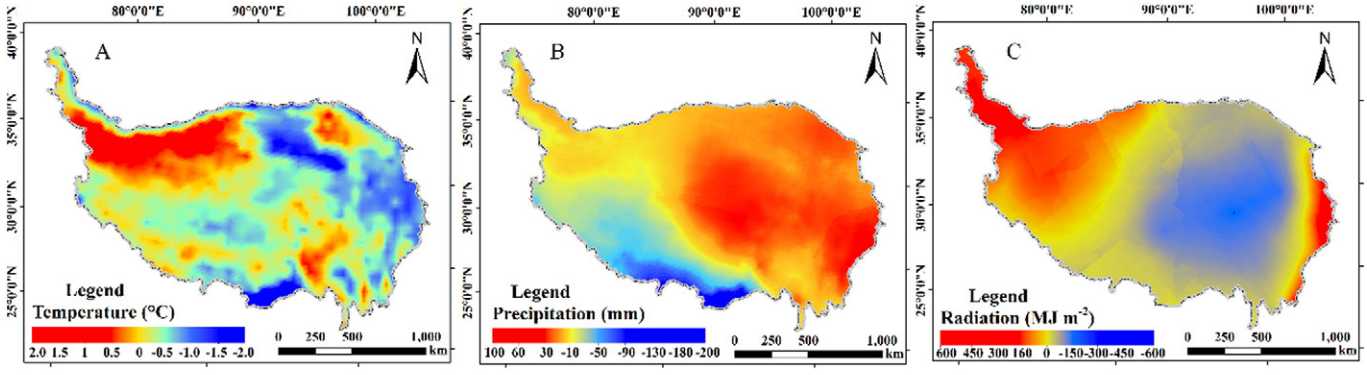

Fig. 6. The change trend of climate factors from 2001 to 2013 in QTP (A, B and C are temperature, precipitation and radiation, respectively).

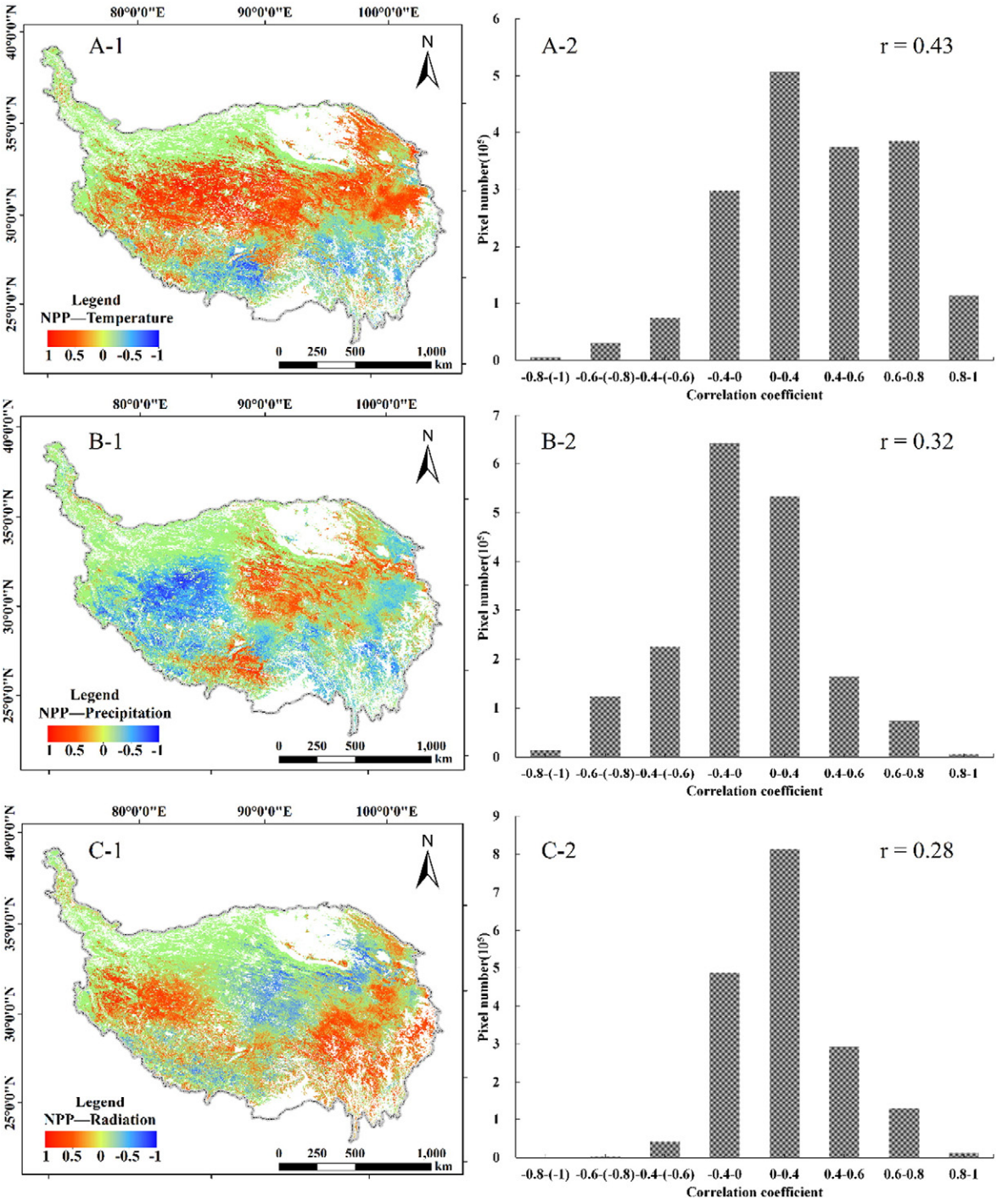

Fig. 7. The spatial distribution and pixel frequency of correlation coefficient between NPPA and influence factors (A-1, B-1 C-1 and D-1 are the correlation coefficient spatial distribution and A-2, B-2, C-2 and D-2 corresponding its pixel frequency.)

radiation during in the same period was approximately 12.5 mm and 12.8 MJ/m^2.

NPP_A was driven by climate factors in this study from 2001 to 2013. Therefore, the correlation coefficient of these factors with NPP was analyzed (Fig. 7). Temperature had the highest average correlation coefficient ($r = 0.43$, $n = 1{,}782{,}912$) of all climate factors (Fig. 7A-1, A-2). Positive correlated areas accounted for 77.2% of the entire region. The southern and southeastern QTP mainly presented a negative correlated with NPP_A. The precipitation in the middle and a part of south of the QTP implied positive relation with NPP_A (Fig. 7B-1, B-2), which occupied 43.6% of the entire region. The west and south of the QTP had a negative contribution to NPP_A, and the average correlation coefficient of the entire region was 0.32. Radiation had the lowest correlation coefficient ($r = 0.28$). However, 70.1% of the region had a positive relation to NPP_A, and most of them ranged from 0 to 0.4 (27.3% of the entire region) (Fig. 7C-1, C-2). Except the middle and the middle north of QTP, the other regions presented positive relation to NPP_A. Overall, temperature had the highest correlation coefficient with NPP_A, and most of the region had a positive contribution to NPP_A.

The correlation analysis indicated that the temperature was the determinant factor in NPP_A dynamics because it had the highest correlation coefficient of all climate factors. The increasing temperature was

Table 4
The dominated climate factor of the typical regions in the QTP (the significant test at the 0.05 level, temp, pre and rad denotes temperature, precipitation and radiation).

No.	Typical region	Longitude	Latitude	Independence test	Stepwise regression	R^2 and significance
1	Gertse	84.274	33.814	Temp & pre (r = −903, sig = 0.000) Rad & pre (r = −0.571, sig = 0.021)	NPP = −0.04 * pre + 98.856	$R^2 = 0.655$, p = 0.001
2	Amdo	90.523	33.351	Temp & pre (r = 0.509, sig = 0.038) Rad & pre (r = −0.503, sig = 0.04)	NPP = 9.516 * temp + 168.783	$R^2 = 0.316$, p = 0.027
3	Chamdo	97.238	31.443	Temp & pre (r = 0.681, sig = 0.012)	NPP = 1.373 * rad − 469.483	$R^2 = 0.548$, p = 0.004
4	Damshung	90.883	30.420	Temp & pre (r = −0.778, sig = 0.01)	NPP = −20.411 * temp + 278.574	$R^2 = 0.575$, p = 0.003
5	Chali	92.956	30.665	Temp & pre (r = 0.493, sig = 0.043) Rad & pre (r = −0.617, sig = 0.012)	NPP = 5.665 * temp + 36.264	$R^2 = 0.551$, p = 0.004
6	Gyatsa	92.712	29.290	Temp & pre (r = −0.905, sig = 0.000)	NPP = −9.610 * temp + 393.61	$R^2 = 0.551$, p = 0.002
7	Gar	80.330	32.010	Temp & pre (r = −0.673, sig = 0.006)	NPP = 2.239 * temp + 50.333	$R^2 = 0.614$, p = 0.002
8	Dirl	93.487	31.442	Temp & pre (r = 0.77, sig = 0.001) Rad & pre (r = −0.663, sig = 0.007)	NPP = 0.952 * rad − 211.025	$R^2 = 0.395$, p = 0.021
9	Rioche	96.403	31.429	Temp & pre (r = 0.716, sig = 0.003)	NPP = 0.688 * rad − 178.387	$R^2 = 0.334$, p = 0.039
10	Lhorong	95.908	30.733	Temp & pre (r = 0.631, sig = 0.01)	NPP = −5.503 * temp + 252.892	$R^2 = 0.317$, p = 0.045
11	Menyuan	101.617	37.383	Temp & pre (r = 0.737, sig = 0.002) Rad & pre (r = −0.524, sig = 0.033)	NPP = −0.39 * pre + 271.639	$R^2 = 0.618$, p = 0.001
12	Henan	101.600	34.733	Independent variable	NPP = −0.391 * pre + 433.518	$R^2 = 0.559$, p = 0.003
13	Nuomuhong	96.417	36.433	Independent variable	NPP = 6.254 * temp + 96.64	$R^2 = 0.654$, p = 0.001
14	Maduo	98.217	34.917	Independent variable	NPP = 26.733 * temp + 201.173	$R^2 = 0.354$, p = 0.032
15	Dari	99.650	33.750	Independent variable	NPP = 0.842 * rad − 258.129	$R^2 = 0.648$, p = 0.017
16	Jiuzhi	101.483	33.433	Independent variable	NPP = −0.222 * pre + 509.877	$R^2 = 0.372$, p = 0.027
17	Qilian	100.250	38.183	Temp & pre (r = 0.758, sig = 0.001) Rad & pre (r = −0.802, sig = 0.000)	NPP = −0.509 * pre + 373.965	$R^2 = 0.605$, p = 0.002
18	Dulan	98.100	36.300	Independent variable	NPP = 0.372 * pre + 131.527	$R^2 = 0.371$, p = 0.027
19	Zadoi	95.300	32.900	Temp & pre (r = 0.881, sig = 0.000) Rad & pre (r = −0.518, sig = 0.035) Rad & temp (r = −0.529, sig = 0.032)	NPP = 9.254 * temp + 339.54	$R^2 = 0.376$, p = 0.026
20	Qumalai	95.783	34.133	Temp & pre (r = 0.893, sig = 0.000) Rad & pre (r = −0.482, sig = 0.048)	NPP = 14.36 * temp + 320.294	$R^2 = 0.465$, p = 0.01

beneficial to vegetation growth (e.g., mid-west of the QTP), but it might lead to droughts (e.g., a part of the northern QTP). The NPP_A was insensitive to the variation in precipitation in the east and mid-west of the QTP because the decreasing or increasing precipitation did not lead to the same trend on NPP_A in the aforementioned region. The radiation related to NPP_A decreased in the east and southeast of the QTP, whereas the temperature and precipitation presented an increasing trend.

We also selected twenty meteorological stations in typical region across the QTP to reveal the effect of climate factors on NPP (Table 4). The temperature, precipitation and radiation of meteorological station were selected as climate variables which in six meteorological stations were independent, the remaining were significantly related. The stepwise regression was established in each typical region because multicollinearity problem exists in the variables. The NPP was significantly related with temperature rather than other variables in ten of the typical regions, and three of them exhibited negative relation with NPP. By contrast, the influence of precipitation on NPP more than other climate factors in six of the typical regions, and five of them significant negative related with NPP. Radiation was the dominated climate factor in four of the typical regions. The results indicated that temperature affected most of the region in the QTP than other climate variables.

3.5. Effect of changing point and seasonal variation of climate variables on NPP

We analyzed the average value of NPP and climate variables, the year of 2008 is the climate change point, the temperature and radiation began to increase while the precipitation decrease sharply after this year (Fig. 8). The variation trend of NPP positive correlated with temperature (Fig. 8A), and tend to negative correlated with precipitation (Fig. 8B). The precipitation reached its maximum value of nearly ten years, the abundant rainfall over the plants' demand, meanwhile, significant increased temperature simulated the growth of vegetation makes the NPP reached a peak in 2009.

The average value of climate forces typically insufficient to present the effect of variables in the process, especially in alpine region (Korner, 2003). The QTP has a unique climate features and sensitive to temperature, then the seasonal change of temperature was investigated to reveal the climate influence on grassland NPP. According to Piao (Piao et al., 2011), March, April and May were defined as spring and June, July and August were summer. We processed the data of 96 meteorological stations in 2001, the result showed that the temperature difference was decreasing while the NPP was increasing across the QTP from north to south (Fig. 9), the precipitation obviously contains two parts, and present from low to high in each part (divided by green line in Fig. 9). The Pearson's correlation coefficient indicates that the temperature difference has a significant negative correlation with NPP, meanwhile, the precipitation was significantly positively correlated with it at the 0.01 level (2-tailed), the rest years also obtained the same results. Therefore, less of the difference in seasonal temperature, the more beneficial to plant growth under precipitation gradients.

4. Discussion

4.1. Merit and limitation of the methodology

Climate and human activities are considered the main driving forces of grassland productivity dynamics. The traditional method depends on field survey or social statistical data to assess the effects of climate and human interference on grassland degradation (Haberl et al., 2007; Rojstaczer et al., 2001). However, this approach is insufficient, particularly in regions where statistical data are lacking or human survey is difficult to perform. The current study used the CASA model (with remote sensing data as input parameters) to simulate actual NPP and potential NPP, and selected it as an indicator to monitor grassland degradation or restoration. The hypothesis is that grassland productivity dynamics are only affected by climate and human activities. The potential NPP is the maximum productivity achieved by the grassland. The difference between potential NPP and actual NPP is only affected by human activities. Unlike the traditional method, the proposed method was able to identify the areas, locations and NPP variations affected by climate and human activities. Furthermore, the advantage of current method is the potential NPP simulation. The previous studies generally applied statistical model to simulate the potential NPP, however, there are numerous

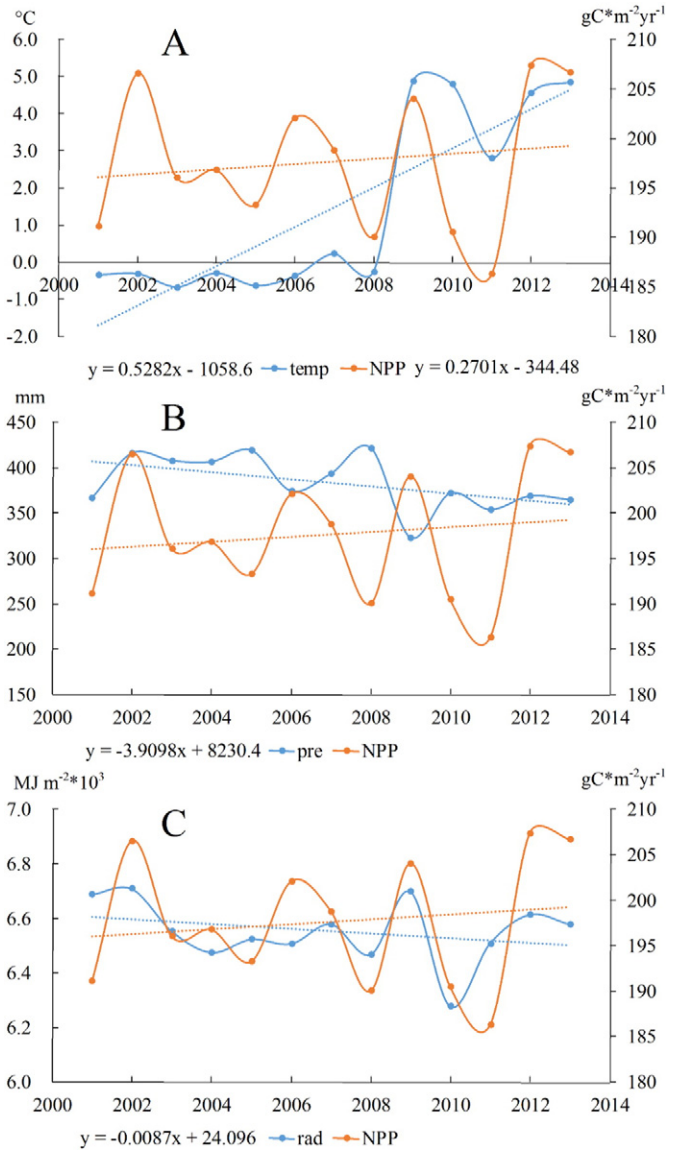

Fig. 8. The NPP dynamics along with the variation of climate factors (A, B and C denote the NPP affected by temperature, precipitation and radiation respectively).

uncertainties remain in statistical model because the only driving parameters are temperature and precipitation. Then the CASA simulated potential NPP has reduced the uncertainty greatly.

Our findings show that 61.2% of the grassland in the QTP experienced a restoration trend, compared with 38.8% of the grassland that experienced a degradation trend during the study period. Climate has a more dominant role in grassland degradation than human activities, which in turn is the dominant force in grassland restoration. The space distribution of the results is inconsistent with the study of Chen (Chen et al., 2014) in the QTP. The difference might be due to the different potential NPP calculation method that was applied in Chen's study. Chen used terrestrial ecosystem model simulated potential NPP by gross primary production minus autotrophic respiration, and actual NPP was simulated by the CASA model. By contrast, this study used the CASA model to simulate potential NPP and actual NPP, except the difference in FPAR. The different study period might be another reason. The study period of Chen was range from 2001 to 2011 compared with the 2001 to 2013 in the current study.

Each method actually has its drawbacks. The potential NPP simulated in the current study indicates that vegetation productivity is achieved under an ideal condition (i.e., only affected by precipitation and air temperature). However, this condition is somehow affected by grassland rodent, grassland fire, and grassland species, vegetation productivity. Similarly, the difference between potential NPP and actual NPP could not only influenced by human interference. All these previously mentioned influencing factors would cause uncertainty to results, it is definitely a challenge to quantitatively assess the influence factors besides climate and human activities. Nevertheless, we differentiate the two main factors in spatial scope at least. Future studies should consider other influential processes.

The land cover change is another important issue in vegetation study. The land cover is strongly affected by global climate and human activities, particularly in the region which climate changed significantly. This study found that the grassland area expanded 6.8% (compared with 2001) according to International Geosphere-Biosphere Program (IGBP) Global vegetation classification scheme map from 2001 to 2013. Therefore, we would miss the driving forces analysis for the expanded grassland region. However, considering the not too long study period, enhance operation efficiency and advantages of GLC2000 classification data, e.g. more grassland types, highest accuracy in four land cover products (IGBP, MODIS and Global Land Cover map produced by the University of Maryland) (Ran et al., 2009), we neglected the uncertain brought by land cover change. However, it must take the effects of land cover change into consideration in a long term study.

4.2. Climate factors on NPP variation

A previous study suggested that precipitation and temperature exhibited an increasing trend (Piao et al., 2011; Piao et al., 2012), given that the current increased rate of temperature nearly doubled that of the last 50 years in the QTP. By contrast, rainfall rate is only one-sixth that of the last 50 years in the QTP (Chen et al., 2014). However, the climate variation is regional, and the average value cannot reflect the real situation of entire region, then we perform the correlation between NPP and climate factors in pixel scale.

The NPP_A and NPP_C have different responses to the climate factors. Temperature is dominant factor in increasing NPP_A, the results were consistent with Gao's study (Gao et al., 2013) in the same place. The temperature and precipitation usually result in a significantly increased NPP (e.g. the northeastern QTP). However, the increasing temperature and decreasing precipitation also could lead to droughts (e.g. the southwestern QTP), the warming and drying phenomenon over QTP would make the grassland ecosystem more sensitive and vulnerable to climate dynamics.

Both of NPP_A and NPP_C are insensitive to precipitation variations. For example, the west of QTP presents a decline in precipitation, whereas NPP did not present the same trend. Precipitation is increased in the eastern and southeastern QTP, but a decreasing trend is identified in this region. The most likely reason would be the melting glaciers have increased runoff in some river systems, providing sufficient water to terrestrial ecosystem. As a result, the glaciers melting process makes the water was more than the plants' demand (Chen et al., 2013). The decline in NPP is more related to the reduction in radiation. Notably, the region where precipitation and radiation decrease, but temperature increases will have less energy input and be drier than before. The warming and drying phenomena in the QTP will lead to grassland degradation more than human activities do.

4.3. Human influence on NPP variation

Our study found that human activities were the dominant factor in grassland restoration, which occupied 39.5% of the total grassland area. Chen (Chen et al., 2014) also indicated that the areas restored by human activities increased from 17.7% (1982 to 2001) to 37.9% (2001 to 2011). The Chinese government has enforced a series of ecological project, such as the Grain to Green Program, which has been

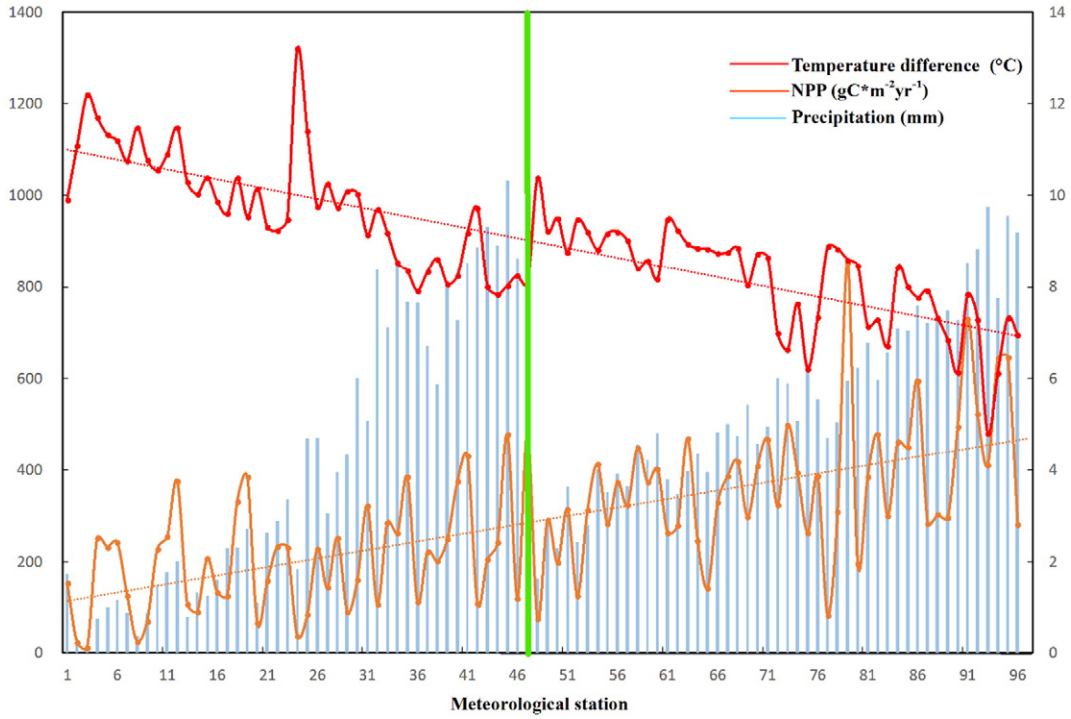

Fig. 9. The temperature difference, precipitation and NPP variation in the QTP.

implemented since 1999, and the Grazing Withdrawal Program, which has been fully implemented since 2002. Livestock also has dramatically decreased since 2004. These projects have achieved productive results in preventing grassland degradation and adjusting forage–livestock balance (Mu et al., 2013). All policies and projects have achieved positive ecological effects and resulted in human activities being the dominant factor in grassland restoration in the QTP.

As we mentioned previously, the degradation was a relative state on the time series. The grassland ecosystem presents a degradation state during the study period, but the results may be different in a longer time series coupled with variations in climate and human activities.

5. Conclusion

This study evaluated the respective contributions of climate and human activities to grassland dynamics in the QTP from 2001 to 2013 by selecting NPP as the indicator and the NPP slope as the basis for scenario simulation. The grassland in the QTP exhibited an increasing trend during the study period.

Nearly 38.8% of the total grassland area decreased by a total of 14,183.8 GgC, whereas 61.2% increased by 15,000.7 GgC. Furthermore, 56.74% and 19.9% of the entire degraded grassland area were induced by climate and human activities, respectively.

The largest area of restoration (accounting for 28.6%) was induced by human activities and exhibited the least increased NPP (5923.4 GgC). By contrast, the areas induced by climate and the combination of the two factors accounted for 12.8% and 19.9% of the restored area, with NPP increases of 3188.1 and 5959.2 GgC respectively.

Overall, climate is the principal driving force of grassland degradation, whereas human activities are the dominant factor in grassland restoration. Furthermore, temperature is dominant factor in climate induced grassland restoration whereas radiation is more related to climate induced grassland degradation. Lastly, the main influential factors may change at different study periods when the driving force of grassland degradation is quantitatively assessed.

Acknowledgments

This work was supported by the "APN Global Change Fund Project (ARCP2014-06NMY-Li & CAF2015-RR14-NMY-Odeh)", the National Natural Science Foundation of China (41271361), the "The Key Project of Chinese National Programs for Fundamental Research and Development (973 Program, 2010CB950702)", "The National High Technology Project (2007AA10Z231)" and the Public Sector Linkages Program supported by Australian Agency for International Development (PSLP: No. 64828). We thank Prof. Jiyuan Liu and Guirui Yu from Institute of geographic sciences and natural resources research, Chinese Academy Science for their guidance on this work. We also thank Ecological environment remote sensing monitoring center of Qinghai province for their help on field survey work.

References

Bartholomé, E., Belward, A.S., 2005. GLC2000: a new approach to global land cover mapping from Earth observation data. Int. J. Remote Sens. 26, 1959–1977.

Chen, H., Zhu, Q., Peng, C., Wu, N., Wang, Y., Fang, X., Gao, Y., Zhu, D., Yang, G., Tian, J., Kang, X., Piao, S., Ouyang, H., Xiang, W., Luo, Z., Jiang, H., Song, X., Zhang, Y., Yu, G., Zhao, X., Gong, P., Yao, T., Wu, J., 2013. The impacts of climate change and human activities on biogeochemical cycles on the Qinghai–Tibetan Plateau. Glob. Chang. Biol. 19, 2940–2955.

Chen, B., Zhang, X., Tao, J., Wu, J., Wang, J., Shi, P., Zhang, Y., Yu, C., 2014. The impact of climate change and anthropogenic activities on alpine grassland over the Qinghai–Tibet Plateau. Agric. For. Meteorol. 189, 11–18.

Conant, R.T., Paustian, K., Elliott, E.T., 2001. Grassland management and conversion into grassland: effects on soil carbon. Ecol. Appl. 11, 343–355.

Fang, J., Liu, G., Xu, S., 1996. Carbon storage in terrestrial ecosystem of China. In: Wang, G.C., Wen, Y.P. (Eds.), The Measurement of Greenhouse Gas and Their Release and Related Processes. China Environmental Science Press, Beijing.

Fassnacht, F.E., Li, L., Fritz, A., 2015. Mapping degraded grassland on the Eastern Tibetan Plateau with multi-temporal Landsat 8 data — where do the severely degraded areas occur? Int. J. Appl. Earth Obs. 42, 115–127.

Gang, C., Zhou, W., Chen, Y., Wang, Z., Sun, Z., Li, J., Qi, J., Odeh, I., 2014. Quantitative assessment of the contributions of climate change and human activities on global grassland degradation. Environ. Earth Sci. 72, 4273–4282.

Gao, Y., Zhou, X., Wang, Q., Wang, C., Zhan, Z., Chen, L., Yan, J., Qu, R., 2013. Vegetation net primary productivity and its response to climate change during 2001–2008 in the Tibetan Plateau. Sci. Total Environ. 444, 356–362.

Genxu, W., Ju, Q., Guodong, C., Yuanmin, L., 2002. Soil organic carbon pool of grassland soils on the Qinghai–Tibetan Plateau and its global implication. Sci. Total Environ. 291, 207–217.
Haberl, H., Erb, K.H., Krausmann, F., Gaube, V., Bondeau, A., Plutzar, C., Gingrich, S., Lucht, W., Fischer-Kowalski, M., 2007. Quantifying and mapping the human appropriation of net primary production in earth's terrestrial ecosystems. Proc. Natl. Acad. Sci. U. S. A. 104, 12942–12945.
Harris, R.B., 2010. Rangeland degradation on the Qinghai–Tibetan plateau: a review of the evidence of its magnitude and causes. J. Arid Environ. 74, 1–12.
Holben, B.N., 1986. Characteristics of maximum-value composite images from temporal AVHRR data. Int. J. Remote Sens. 7, 1417–1434.
Kato, T., Tang, Y., Gu, S., Cui, X., Hirota, M., Du, M., Li, Y., Zhao, X., Oikawa, T., 2004. Carbon dioxide exchange between the atmosphere and an alpine meadow ecosystem on the Qinghai–Tibetan Plateau, China. Agric. For. Meteorol. 124, 121–134.
Korner, C., 2003. Alpine Plant Life: Functional Plant Ecology of High Mountain Ecosystems. Springer.
Li, B., 1997. The degradation of grassland in North China and its countermeasure. Sci. Agric. Sin. 30.
Li, A., Wu, J., Huang, J., 2012. Distinguishing between human-induced and climate-driven vegetation changes: a critical application of RESTREND in inner Mongolia. Landsc. Ecol. 27, 969–982.
Mu, S., Zhou, S., Chen, Y., Li, J., Ju, W., Odeh, I.O.A., 2013. Assessing the impact of restoration-induced land conversion and management alternatives on net primary productivity in inner Mongolian grassland, China. Glob. Planet. Chang. 108, 29–41.
Nan, Z., 2005. The grassland farming system and sustainable agricultural development in China. Grassl. Sci. 51, 15–19.
Piao, S., Fang, J., Zhou, L., Ciais, P., Zhu, B., 2006. Variations in satellite-derived phenology in China's temperate vegetation. Glob. Chang. Biol. 12, 672–685.
Piao, S., Fang, J., Ciais, P., Peylin, P., Huang, Y., Sitch, S., Wang, T., 2009. The carbon balance of terrestrial ecosystems in China. Nature 458, 1009–U1082.
Piao, S., Cui, M., Chen, A., Wang, X., Ciais, P., Liu, J., Tang, Y., 2011. Altitude and temperature dependence of change in the spring vegetation green-up date from 1982 to 2006 in the Qinghai-Xizang Plateau. Agric. For. Meteorol. 151, 1599–1608.
Piao, S., Tan, K., Nan, H., Ciais, P., Fang, J., Wang, T., Vuichard, N., Zhu, B., 2012. Impacts of climate and CO2 changes on the vegetation growth and carbon balance of Qinghai–Tibetan grasslands over the past five decades. Glob. Planet. Chang. 98–99, 73–80.
Potter, C.S., Randerson, J.T., Field, C.B., Matson, P.A., Vitousek, P.M., Mooney, H.A., Klooster, S.A., 1993. Terrestrial ecosystem production — a process model-based on global satellite and surface data. Glob. Biogeochem. Cycles 7, 811–841.
Potter, C.S., Klooster, S., Brooks, V., 1999. Interannual variability in terrestrial net primary production: exploration of trends and controls on regional to global scales. Ecosystems 2, 36–48.
Qiu, J., 2008. The third pole. Nature 454, 393–396.
Rahimi, S., Sefidkouhi, M.A.G., Raeini-Sarjaz, M., Valipour, M., 2015. Estimation of actual evapotranspiration by using MODIS images (a case study: Tajan catchment). Arch. Agron. Soil Sci. 61, 695–709.
Ran, Y.H., Xin, L.I., Ling, L.U., 2009. Accuracy evaluation of the four remote sensing based land cover products over China. J. Glaciol. Geocryol.
Rojstaczer, S., Sterling, S.M., Moore, N.J., 2001. Human appropriation of photosynthesis products. Science 294, 2549–2552.
Scurlock, J.M.O., Hall, D.O., 1998. The global carbon sink: a grassland perspective. Glob. Chang. Biol. 4, 229–233.
Tan, K., Ciais, P., Piao, S., Wu, X., Tang, Y., Vuichard, N., Liang, S., Fang, J., 2010. Application of the ORCHIDEE global vegetation model to evaluate biomass and soil carbon stocks of Qinghai–Tibetan grasslands. Glob. Biogeochem. Cycles 24, GB1013.
Valipour, M., 2015a. Comparative evaluation of radiation-based methods for estimation of potential evapotranspiration. J. Hydrol. Eng. 20.
Valipour, M., 2015b. Evaluation of radiation methods to study potential evapotranspiration of 31 provinces. Meteorog. Atmos. Phys. 127, 289–303.
Valipour, M., 2015c. Investigation of Valiantzas' evapotranspiration equation in Iran. Theor. Appl. Climatol. 121, 267–278.
Valipour, M., 2015d. Study of different climatic conditions to assess the role of solar radiation in reference crop evapotranspiration equations. Arch. Agron. Soil Sci. 61, 679–694.
Valipour, M., Eslamian, S., 2014. Analysis of potential evapotranspiration using 11 modified temperature-based models. Int. J. Hydrol. Sci. Technol. 4.
Wang, G., Liu, L.a., Liu, G., Hu, H., Li, T., 2010. Impacts of grassland vegetation cover on the active-layer thermal regime, northeast Qinghai–Tibet Plateau, China. Permafr. Periglac. 21, 335–344.
Wessels, K.J., Prince, S.D., Frost, P.E., van Zyl, D., 2004. Assessing the effects of human-induced land degradation in the former homelands of northern South Africa with a 1 km AVHRR NDVI time-series. Remote Sens. Environ. 91, 47–67.
Wessels, K.J., Prince, S.D., Reshef, I., 2008. Mapping land degradation by comparison of vegetation production to spatially derived estimates of potential production. J. Arid Environ. 72, 1940–1949.
Xiao, X., Zhang, Q., Hollinger, D., Aber, J., Iii, B.M., 2005. Modeling gross primary production of an evergreen needleleaf forest using Modis and climate data. Ecol. Appl. 15, 954–969.
Xu, D.Y., Kang, X.W., Liu, Z.L., Zhuang, D.F., Pan, J.J., 2009. Assessing the relative role of climate change and human activities in sandy desertification of Ordos region, China. Sci. China Ser D 52, 855–868.
Yu, C., Zhang, Y., Claus, H., Zeng, R., Zhang, X., Wang, J., 2012. Ecological and environmental issues faced by a developing Tibet. Environ. Sci. Technol. 1979–1980.
Zhao, L., Li, Y., Xu, S., Zhou, H., Gu, S., Yu, G., Zhao, X., 2006. Diurnal, seasonal and annual variation in net ecosystem CO2 exchange of an alpine shrubland on Qinghai–Tibetan plateau. Glob. Chang. Biol. 12, 1940–1953.
Zheng, D., 1996. The system of physico-geographical regions of the Qinghai-Xizang (Tibet) Plateau. Sci. China 4, 410–417.
Zhou, W., Gang, C., Zhou, F., Li, J., Dong, X., Zhao, C., 2015. Quantitative assessment of the individual contribution of climate and human factors to desertification in northwest China using net primary productivity as an indicator. Ecol. Indic. 48, 560–569.
Zhu, W.Q., Pan, Y.Z., He, H., Yu, D.Y., Hu, H.B., 2006. Simulation of maximum light use efficiency for some typical vegetation types in China. Chin. Sci. Bull. 51, 457–463.